IOPscience iopscience.iop.org

Home Search Collections Journals About Contact us My IOPscience

Evolution of the dendritic morphology with the solidification velocity in rapidly solidified Al-4.5wt.%Cu droplets

This content has been downloaded from IOPscience. Please scroll down to see the full text.

2015 IOP Conf. Ser.: Mater. Sci. Eng. 84 012016

(http://iopscience.iop.org/1757-899X/84/1/012016)

View the table of contents for this issue, or go to the journal homepage for more

Download details:

IP Address: 147.94.212.92
This content was downloaded on 23/11/2015 at 09:42

Please note that terms and conditions apply.

Evolution of the dendritic morphology with the solidification velocity in rapidly solidified Al-4.5wt.%Cu droplets

M Bedel[1], G Reinhart[1], Ch-A Gandin[2], A-A Bogno[3], H Nguyen-Thi[1], H Henein[3]
[1] Aix-Marseille University & CNRS, IM2NP UMR 7334, Campus Saint-Jérôme, Case 142, 13397 Marseille Cedex 20, France
[2] MINES ParisTech & CNRS, CEMEF UMR 7635, 06904 Sophia Antipolis, France
[3] AMPL, Department of Chemical and Materials Engineering, University of Alberta, Canada

E-mail: marie.bedel@im2np.fr

Abstract. The microstructure morphology of Al-4.5wt.%Cu droplets formed by the Impulse Atomization technique is investigated. Three-dimensional reconstructions by synchrotron X-ray micro-tomography of several droplets reveal different morphologies in droplets of similar diameter and produced in the same batch. Moreover, microstructural features also indicate that the development of the dendrite arms occurs in some droplets along <111> crystallographic axes instead of the usual <100> directions observed in conventional casting for the same alloy. It has been observed that such an unusual growth direction of the dendrites is directly related to the solidification velocity. We underpin these results by carrying out comparisons with a solidification model. Predictions are used to discuss the change of dendrite growth direction, as well as the existence of a dendrite growth direction range for a given type of droplets. In addition, the effect of the droplet size and the cooling gas on the dendrite growth direction range observed experimentally is also investigated by using the model.

1. Introduction

Rapid solidification techniques have been developed as they enable to obtain a wide variety of structures which cannot be formed under conventional solidification processes [1]. They differ by the way to form the liquid as a strip or a droplet and by the method of heat extraction. Atomization techniques are used to make metallic powders which are used for making a desired object by pressing or by sintering [2]. The liquid metal generated as a stream breaks up into droplets by Rayleigh-Plateau instability, which subsequently solidify in a much colder medium. In the Impulse Atomization (IA) technique the liquid is pushed through a nozzle plate to form the liquid streams [3].

In order to deepen the understanding of the microstructure formation in the droplets, synchrotron X-ray micro-tomography was carried out at the European Synchrotron Radiation Facility (ESRF, Grenoble, France). Three-dimensional reconstructions of a large number of droplets were obtained, enabling the inner microstructure of the droplets to be statistically analysed for the first time. In a previous paper, we showed that four distinct morphologies could be identified in droplets of the same size and from the same batch [4]. Such a range of morphologies can be linked to a range of solidification velocities for the droplets. Indeed, while Rappaz and co-workers highlighted the <100>

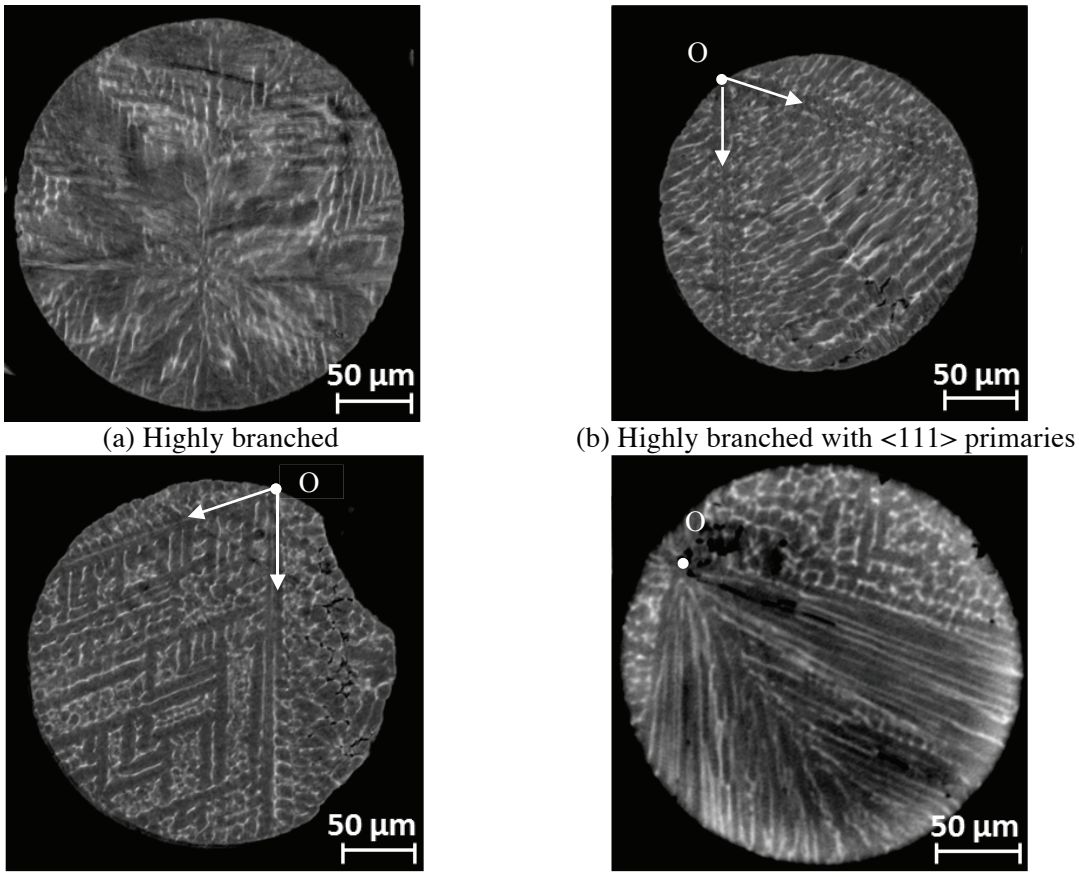
[1] marie.bedel@im2np.fr

Content from this work may be used under the terms of the Creative Commons Attribution 3.0 licence. Any further distribution of this work must maintain attribution to the author(s) and the title of the work, journal citation and DOI.
Published under licence by IOP Publishing Ltd

to <110> continuous transition induced by the solute composition variation in Al-Zn alloys [5], the work of Chan and co-workers [6] and Gudgel et al. [7] on NH_4-Cl and more recently the work of Castle et al. on Cu-Ni [8] and Chen et al. on Al-Fe [9] showed that the growth orientation transition from <100> to <111> occurs when the solidification velocity increases.
The purpose of the present study is to use a solidification model [10] [11] to get a better understanding of the experimental observations. Although the model does not provide direct information on the growth orientation of the grain microstructure, the final morphologies of the droplet can be linked to the evolution of the predicted growth velocity. Moreover, the impact of the droplet size and the cooling gas on the predicted solidification velocity is also compared to experimental observations.

2. Experimental and modelling details

This study focuses on Al-4.5wt.%Cu droplets, as this alloy has already been considered in previous works on powder atomization [11][12]. The droplets are formed by the IA technique [3]. Its principle is as follows: the alloy, melted in a furnace, is then pushed through a nozzle plate by mechanical impulses. The resulting liquid jets break into small droplets due to the Rayleigh-Plateau instability. While falling through a stagnant atmosphere of argon or helium gas, the droplets lose their heat and solidify. When they reach the oil quench bath placed 4 meters below, they are already fully solid. This technique leads to a size distribution of the droplets, whose diameter can vary from less than 200 μm to more than 1 mm in the same batch. The droplets are then sieved into several size classes by the technique described in [13].
Once the droplets are formed and sieved, their microstructure morphology is investigated for different size ranges and for the two cooling gases. For this purpose, synchrotron X-ray micro-tomography is used post-mortem [14]. This technique provides a three-dimensional reconstruction of the droplets where the grey level depends on the X-ray transmission of the phase. The primary phase (Al) being less absorbing than the eutectic (Al+Al_2Cu), the last formed solid appears in lighter grey in the tomography reconstructions. The image acquisition and the 3-D reconstruction were performed on the ID19 beamline at the ESRF. The resolution is 0.56 μm/pixel (field of view of 1146 μm), which enables us to study several small droplets at once. The statistical analysis of the droplet morphology has be carried out using ImageJ software [15]. The final droplet microstructure is the result of a complex three dimensional competition between dendrite arms. Therefore we only consider for this study the cross-sections showing characteristic morphologies, as shown in Figure 1, where the four distinct morphologies observed in the hundred-plus studied droplets are represented.
Droplet solidification is predicted by a solidification model detailed in [10]. The volume-averaged mass conservation equations are written and solved with limited diffusion in all phases as in standard microsegregation analyses. Even though coupling with a heat balance is made, a uniform temperature is assumed in the droplet. The heat extraction rate is computed thanks to an atomization model [12]. The solidification model also accounts for nucleation undercooling of the phases and the growth kinetics of the dendritic and eutectic microstructures [11][12]. It predicts the time evolution of temperature, volume fraction and solute composition of the phases. In the model, a single nucleation event per phase is assumed to take place at the centre of a spherical droplet. Also reaction for each successive microstructure is approximated by radial growth in the droplet.



(a) Highly branched (b) Highly branched with <111> primaries

(c) Dendritic (d) Finger bundle

Figure 1. Examples of the four morphologies identified in the Al-4.5wt.%Cu droplets of diameter between 250 and 300 μm: (a) highly branched morphology, (b) highly branched morphology with visible primary arms oriented along <111> directions, (c) dendritic morphology and (d) finger bundle morphology. The nucleation position noted O is shown by a white dot and the primary arms by white arrows.

For all calculations, the Al-Cu phase diagram and the phase enthalpy and equilibrium composition are taken from the PBIN thermodynamic database [16]. Properties such as the liquidus slope and the partition coefficient thus vary with temperature and composition. The elements densities are taken from [17] and the solute diffusion coefficients in the solid and liquid phases from [18] and [19], respectively. They depend on the temperature as $D=D_0.\exp(-Q/RT)$ with R the molar gas constant. The Gibbs-Thomson coefficients for the primary Al-rich phase and the Al_2Cu phase are given in [20] and the Al-rich/liq and Al_2Cu/liq contact angles in [21]. The secondary dendrite arm spacing is obtained by linear interpolation of the experimental measurements from tomography analyses. For droplets solidified in argon, $\lambda_2 = 4.5017 + 0.0149 \times d$ and in helium, $\lambda_2 = - 0.4902 + 0.0224 \times d$, where d is the droplet diameter in microns. The process parameters used by default in the present calculations are given in Table 1.

Table 1: Default parameters values used in the simulations

Alloy parameters	Value	Unit
Phase diagram	PBIN [16]	
Density	2982	$kg.m^{-3}$
Diffusion coefficient of Cu		
solid Al-rich phase D_0^s	$6.47x10^{-5}$	$m^2.s^{-1}$
liquid D_0^l	$1.05x10^{-7}$	$m^2.s^{-1}$
solid Al-rich phase Q^s	135000	$J.mol^{-1}$
liquid Q^l	23804	$J.mol^{-1}$
Gibbs-Thomson coefficients		
solid Al-rich/liquid interface	$2.41x10^{-7}$	m.K
solid Al_2Cu/liquid interface	$0.55x10^{-7}$	m.K

Process parameters	Value	Unit
Alloy composition in copper	4.5	wt.%
Gas temperature	293	K
Initial droplet velocity	0.5	$m.s^{-1}$
Initial droplet temperature	933	K
Nucleation undercooling	5	K
Droplet diameter	300	μm

3. Results and discussion

3.1. Dendrite growth direction evolution

A major result of the synchrotron X-ray micro-tomography analysis is the variety of dendrite morphologies for droplets solidifying under the same process conditions. These morphologies have been described in details in [4] by combining electron backscatter diffraction (EBSD) and X-ray micro-tomography analysis. We only remind here their main characteristics. Some of the droplets grow in the usual <100> directions and present a highly branched microstructure, as illustrated in Figure 1-a. A structure growing first in <111> directions and then in <100> directions can also be observed as in Figure 1-b. The two other types of morphologies are fully growing along <111> directions, with a dendritic (Figure 1-c) or a finger-bundle morphology (Figure 1-d).

In order to explain the growth direction change from <111> to <100> observed in some droplets (Figure 1-b), we consider the growth kinetics predicted by the model for a 300 μm diameter droplet solidifying in argon. The time-evolution of the temperature T and the dendrite tip growth velocity v_{tip} are shown in Figure 2-a. The simulation enables the distinction of different growth regimes. Firstly, the temperature continuously decreases after reaching the nucleation temperature (imposed through the nucleation undercooling ΔT_n). After nucleation, the dendrite tip growth velocity increases very rapidly until the beginning of recalescence (t=0.0154s indicated by the vertical dashed line in Figure 2-a). Then, the heat released by the solidification more than compensates the heat extracted from the droplet and the temperature increases while the overall solid fraction still increases in the droplet. As the calculated average liquid composition does not increase yet, the liquidus temperature does not vary significantly. Thus the undercooling, which is the driving force for the growth, decreases as the temperature increases and the dendrite tip velocity decreases accordingly. In a second step, an almost permanent regime is reached where the temperature and the growth velocity tend to stabilize. Finally, when the grain envelope approaches the droplet periphery, the solute enrichment of the extra-dendritic liquid is not negligible anymore and growth is slowed down. From this time ($t \approx 0.075$s), we observe

that the solid fraction evolution approaches the Gulliver-Scheil approximation as diffusion in the solid phase is limited and solute is well mixed in the liquid phase.
These different growth regimes can explain the dendrite growth direction change observed in droplets by considering that the growth orientation is linked to the growth velocity. Indeed, the first solid that forms very fast can grow along the <111> directions if its growth velocity reaches values beyond the growth orientation transition. Then the growth velocity decreases and the last part of the droplet would grow in the <100> directions, as observed Figure 1-b.

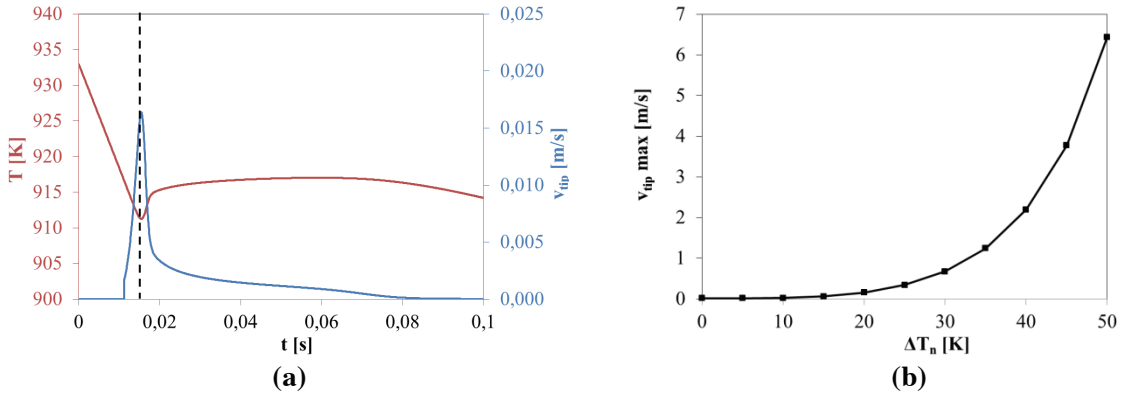


Figure 2. (a) Predicted time evolution of temperature and tip velocity during the solidification beginning of a droplet cooled in argon whose diameter is equal to 300μm, for a nucleation undercooling fixed at ΔT_n=5°C. The dashed line corresponds to both the maximal tip velocity and the local minimum temperature and (b) Predicted maximal tip velocity reached during solidification of a droplet cooled in argon whose diameter is equal to 300μm, depending on the imposed nucleation undercooling value.

3.2. Dendrite growth direction distribution
The previous analysis of the droplet growth kinetics is not sufficient to explain why droplets solidified under the same conditions in the same batch reveal the diverse oriented microstructures shown in Figure 1. The four morphologies are indeed found in similar proportions for 40 droplets of the same batch and whose diameter is between 250 and 300 μm, as can be seen further in Figure 3. While their cooling history can be considered as similar in a first approximation, we actually have no precise information on the temperature of the nucleation event in each droplet. An average nucleation temperature can be estimated through the secondary dendrite arm spacing and the eutectic fraction for a range of droplets by the technique developed in [22]. However, a range of nucleation temperature can exist. Therefore, we varied the nucleation undercooling ΔT_n in the model from 0°C to 50°C to look at its impact on the growth velocity during the droplet solidification. When ΔT_n is increased, the start of the growth is delayed but the initial driving force for growth is higher. This explains why the maximum velocity is multiplied by almost a factor 400 when ΔT_n is increased from 5°C to 50°C, as can be seen in Figure 2-b. It is also worth noting that varying ΔT_n only impacts the solidification start as the solidification tends to follow very rapidly the Gulliver-Scheil model afterwards. Although we do not know a priori the growth velocity limit inducing the growth orientation change, we can see that the higher ΔT_n is, the faster the first solid is formed and the larger the fraction of rapidly formed solid would be. Thus, the temperature of the nucleation event can significantly alter the kinetics of the droplet solidification and as a consequence the growth orientation of the microstructure. A range of nucleation undercooling could therefore help explain the variety of dendrite growth directions observed in droplets solidified under the same process conditions.

3.3. Effect of droplet size

The previous comparison between experimental observations and the numerical simulations was made for a given size of droplet. We also observe from the synchrotron X-ray micro-tomography data analysis that the droplet size has a strong impact on the microstructure distribution. Indeed, the 4 dendrite morphologies are almost identically represented in droplets of diameter 250 μm < d < 300 μm, while <111> oriented microstructures are more present in smaller droplets of diameter 0 μm < d < 212 μm, as shown in Figure 3.

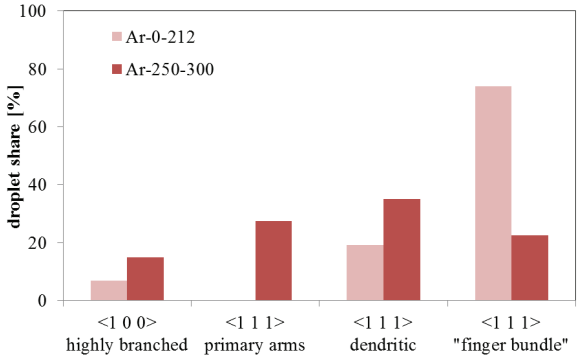


Figure 3: Droplet share of the four morphologies for the droplets solidified in argon which diameter is between 0 and 212 μm (73 droplets) and between 250 and 300 μm (40 droplets).

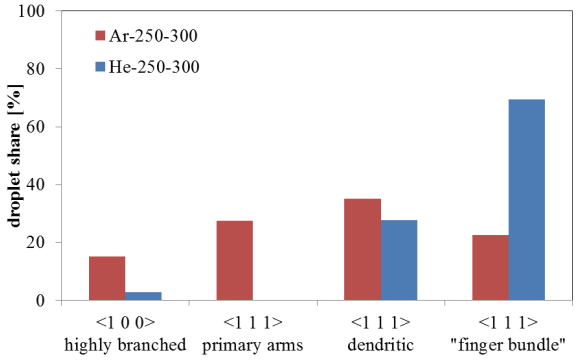


Figure 4: Droplet share of the four morphologies for droplets which diameter is between 250 and 300 μm, solidified in argon (40 droplets) and in helium (36 droplets).

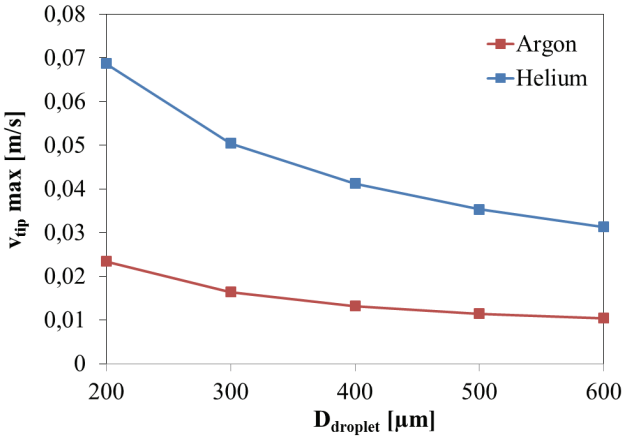


Figure 5: Impact of cooling gas and droplet diameter on the maximal tip velocity, for a nucleation undercooling equal to 5°C.

The impact of the droplet size on the maximum predicted velocity is illustrated in Figure 5. The predicted maximum dendrite velocity is almost doubled when the droplet diameter decreases from 600 μm to 200 μm, independently of the cooling gas, as the tendency is observed for droplets solidified in argon (red curve) as for droplets solidified in helium (blue curve). Figure 5 compiles results for an imposed nucleation undercooling ΔT_n=5°C but the tendency was found identical for a range of nucleation undercoolings from 0°C to 50°C. Thus, according to the model, the intensity of the rapid solidification step increases significantly when the droplet size decreases, for the two tested cooling gases and for a range of nucleation undercoolings. This can explain the promotion of the fully <111> growth orientation for smaller droplets, observed experimentally (Figure 3). In addition, we can note that mostly <111> growth orientation is obtained for the 0-212 μm diameter droplets

3.4. Effect of cooling gas

The impact of the cooling gas has also been investigated by considering droplets cooled in argon and helium atmospheres. The micro-tomography analysis shows that, all others parameters being similar, the <111> finger bundle morphology is promoted in helium in comparison with argon, as illustrated in Figure 4. As shown in Figure 5, much larger maximum growth velocities during the rapid solidification step are predicted by the model for droplets solidified in helium, all other parameters being equal. This trend is actually the same for the range of nucleation undercooling and droplet diameter investigated in the present study. Since the thermal conductivity of helium is more than 8 times larger than the one of argon, the heat extraction of the droplet is much faster when cooled in helium atmosphere. The intensity of the rapid solidification step is then larger for droplets solidified in helium, which is in agreement with the fact that the <111> finger bundle morphology is more represented in this case.

4. Conclusion

We have studied the microstructure and more precisely the dendrite growth direction of droplets formed by the IA technique using synchrotron X-ray micro-tomography. Droplets formed under the same process conditions and with the same size have different morphologies. By statistical analysis, we could estimate the morphology distribution of the droplets for different droplets sizes and for two cooling gases. The impact of the nucleation undercooling, droplet size and cooling gas are discussed based on simulations with a solidification model. We have showed that the observed experimental trend can be retrieved using the model assuming that the dendrite growth direction can change from <100> to <111> if the solidification velocity becomes large enough.

However, a more precise model accounting for the anisotropy of interfacial free energy and the anisotropy of attachment kinetics is needed to directly link the dendrite growth direction in a droplet to its solidification velocity. To this, a phase field model is also currently under development.

5. Acknowledgements

This study has been performed in the framework of MIMOSA project funded by the French National Research Agency (ANR) in collaboration with the Natural Sciences and Engineering Research Council of Canada. The authors would like to thank Gildas Guillemot from CEMEF for fruitful discussions.

References

[1] Jones H 1984 *J. Mater. Sci.* **19** 1043–76
[2] Prasad A 2006 *PhD Thesis* 70
[3] Henein H 2002 *Mater. Sci. Eng. A* **326** 92–100
[4] Bedel M, Reinhart G, Bogno A-A, Gandin C-A, Jacomet S, Boller E, Nguyen-Thi H and Henein H 2015 *Acta Mater.* **89** 234–46
[5] Haxhimali T, Karma A, Gonzales F and Rappaz M 2006 *Nat. Mater.* **5** 660–4
[6] Chan S-K, Reimer H-H and Kahlweit M 1976 *J. Cryst. Growth* **32** 303–15
[7] Gudgel K A and Jackson K A 2001 *J. Cryst. Growth* **225** 264–7
[8] Castle E G, Mullis A M and Cochrane R F 2014 *Acta Mater.* **66** 378–87
[9] Chen J, Dahlborg U, Bao C M, Calvo-Dahlborg M and Henein H 2011 *Metall. Mater. Trans. B* 1–11
[10] Tourret D and Gandin C-A 2009 *Acta Mater.* **57** 2066–79
[11] Prasad A, Mosbah S, Henein H and Gandin C-A 2009 *ISIJ Int.* **49** 992–9
[12] Wiskel J B, Henein H and Maire E 2002 *Can. Metall. Q.* **41** 97–110
[13] Federation M P I 2012 (S.l.: Metal Powder Industry)
[14] Nguyen-Thi H, Salvo L, Mathiesen R H, Arnberg L, Billia B, Suery M and Reinhart G 2012 *Comptes Rendus Phys.* **13** 237–45
[15] Abramoff M D, Magalhães P J and Ram S J 2004 *Biophotonics Int.* **11** 36–42

[16] PBIN, TCS thermodynamic database v1.2, Thermo-Calc Software AB, 2008 (Stockholm, SE)
[17] Totemeier W F G C 2004 *Smithells Metals Reference Book (Eighth Edition)* (Oxford: Butterworth-Heinemann) pp 1–27
[18] Heringer R, Gandin C-A, Lesoult G and Henein H 2006 *Acta Mater*. **54** 4427–40
[19] Du Y, Chang Y A, Huang B, Gong W, Jin Z, Xu H, Yuan Z, Liu Y, He Y and Xie F-Y 2003 *Mater. Sci. Eng. A* **363** 140–51
[20] Kurz W and Fisher D 1986 (4711, Aedermannsdorf, Switzerland: Trans Tech Publications Ltd, Trans Tech House)
[21] Gandin C-A, Mosbah S, Volkmann T and Herlach D M 2008 *Acta Mater*. **56** 3023–35
[22] Bogno A-A, Delshad Khatibi P, Henein H and Gandin C-A 2013 *Materials Science & Technology Conference and Exhibition 2013* vol 2 (Montreal, QC, Canada) pp 1153–60